

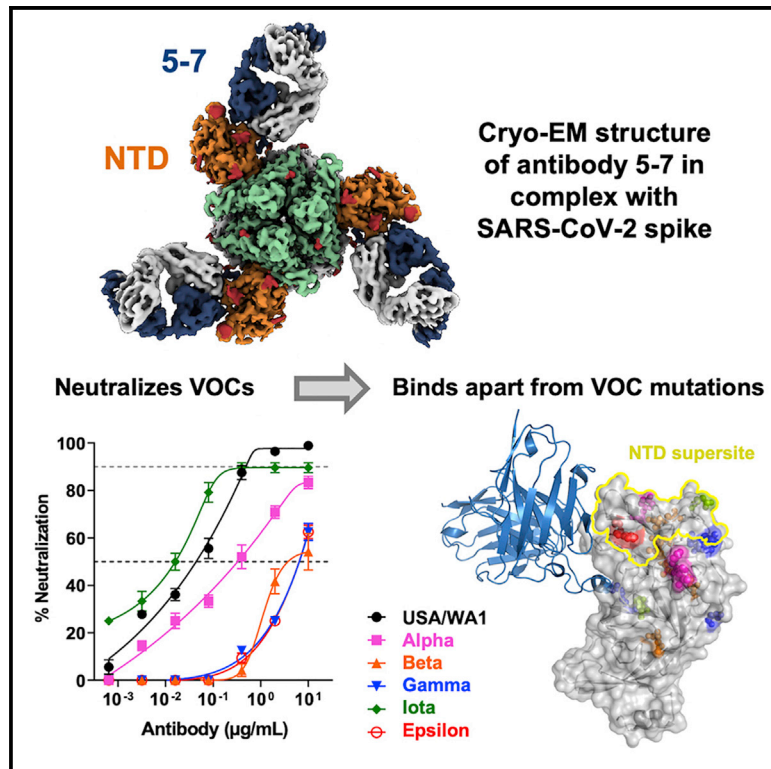


Since January 2020 Elsevier has created a COVID-19 resource centre with free information in English and Mandarin on the novel coronavirus COVID-19. The COVID-19 resource centre is hosted on Elsevier Connect, the company's public news and information website.

Elsevier hereby grants permission to make all its COVID-19-related research that is available on the COVID-19 resource centre - including this research content - immediately available in PubMed Central and other publicly funded repositories, such as the WHO COVID database with rights for unrestricted research re-use and analyses in any form or by any means with acknowledgement of the original source. These permissions are granted for free by Elsevier for as long as the COVID-19 resource centre remains active.

Neutralizing antibody 5-7 defines a distinct site of vulnerability in SARS-CoV-2 spike N-terminal domain

Graphical abstract



Authors

Gabriele Cerutti, Yicheng Guo, Pengfei Wang, ..., David D. Ho, Zizhang Sheng, Lawrence Shapiro

Correspondence

dh2994@cumc.columbia.edu (D.D.H.),
zs2248@cumc.columbia.edu (Z.S.),
lss8@columbia.edu (L.S.)

In brief

Cerutti et al. report the cryo-EM structure of potent neutralizing antibody 5-7 bound to SARS-CoV-2 spike. While most NTD-directed neutralizing antibodies target the NTD supersite, 5-7 binds to a conserved hydrophobic pocket on NTD and neutralizes many variants of concern.

Highlights

- Cryo-EM structure of neutralizing antibody 5-7 in complex with SARS-CoV-2 spike
- 5-7 recognizes NTD outside of the previously identified antigenic supersite
- 5-7 binds to a site known to accommodate numerous hydrophobic ligands
- Structural basis of 5-7 neutralization tolerance to some variants of concern



Report

Neutralizing antibody 5-7 defines a distinct site of vulnerability in SARS-CoV-2 spike N-terminal domain

Gabriele Cerutti,^{1,5} Yicheng Guo,^{2,5} Pengfei Wang,² Manoj S. Nair,² Maple Wang,² Yaoxing Huang,² Jian Yu,² Lihong Liu,² Phinikoula S. Katsamba,¹ Fabiana Bahna,¹ Eswar R. Reddem,¹ Peter D. Kwong,^{3,4} David D. Ho,^{2,*} Zizhang Sheng,^{2,*} and Lawrence Shapiro^{1,2,3,4,6,*}

¹Zuckerman Mind Brain Behavior Institute, Columbia University, New York, NY 10027, USA

²Aaron Diamond AIDS Research Center, Columbia University Vagelos College of Physicians and Surgeons, New York, NY 10032, USA

³Department of Biochemistry and Molecular Biophysics, Columbia University, New York, NY 10032, USA

⁴Vaccine Research Center, National Institute of Allergy and Infectious Diseases, National Institutes of Health, Bethesda, MD 20892, USA

⁵These authors contributed equally

⁶Lead contact

*Correspondence: dh2994@cumc.columbia.edu (D.D.H.), zs2248@cumc.columbia.edu (Z.S.), lss8@columbia.edu (L.S.)
<https://doi.org/10.1016/j.celrep.2021.109928>

SUMMARY

Antibodies that potently neutralize SARS-CoV-2 target mainly the receptor-binding domain or the N-terminal domain (NTD). Over a dozen potently neutralizing NTD-directed antibodies have been studied structurally, and all target a single antigenic supersite in NTD (site 1). Here, we report the cryo-EM structure of a potent NTD-directed neutralizing antibody 5-7, which recognizes a site distinct from other potently neutralizing antibodies, inserting a binding loop into an exposed hydrophobic pocket between the two sheets of the NTD β sandwich. Interestingly, this pocket was previously identified as the binding site for hydrophobic molecules, including heme metabolites, but we observe that their presence does not substantially impede 5-7 recognition. Mirroring its distinctive binding, antibody 5-7 retains neutralization potency with many variants of concern (VOCs). Overall, we reveal that a hydrophobic pocket in NTD proposed for immune evasion can be used by the immune system for recognition.

INTRODUCTION

Severe acute respiratory syndrome-coronavirus-2 (SARS-CoV-2), the causative agent for coronavirus disease 2019 (COVID-19), emerged in 2019, leading to the ongoing worldwide pandemic, which has led to several million deaths (Callaway et al., 2020; Cucinotta and Vanelli, 2020; Dong et al., 2020). Hundreds of millions of COVID-19 cases have been reported, giving ample opportunity for the emergence of mutants, and numerous variants of concern (VOCs), including alpha (B.1.1.7), beta (B.1.351), gamma (P.1), delta (B.1.617.2), epsilon (B.1.427/9), and iota (B.1.526), have become dominant in some geographic regions and are now driving the pandemic (Annavajhala et al., 2021; Faria et al., 2021; Tang et al., 2021; Tegally et al., 2020; Yadav et al., 2021; Zhang et al., 2021). Numerous mutations in circulating VOCs are within the epitopes of neutralizing antibody classes common in the convalescent human repertoire, consistent with their selection in response to human immune pressure (Cerutti et al., 2021b; Rapp et al., 2021; Yuan et al., 2020). While effective vaccines are now being widely distributed in some countries, the pace and geographic restriction of vaccine administration ensures the continued rise of new infections and the continued need for therapeutics.

One promising therapeutic approach, the identification of SARS-CoV-2-neutralizing antibodies that could be used as therapeutic or prophylactic agents, has been extensively explored. The primary target for neutralizing antibodies is the viral spike protein, a trimeric type I viral fusion machine (Walls et al., 2020; Wrapp et al., 2020b) that allows the virus to bind to the angiotensin converting enzyme 2 (ACE2) receptor on host cells through its receptor-binding domain (RBD) (Benton et al., 2020; Yan et al., 2020; Zhou et al., 2020) and mediates fusion between the viral and cell membranes. The spike protein comprises two subunits: the S1 subunit comprising the N-terminal domain (NTD), RBD, and several other subdomains, and the S2 subunit that mediates virus-cell membrane fusion (Walls et al., 2020; Wrapp et al., 2020b). The majority of SARS-CoV-2 neutralizing antibodies so far identified target RBD (Brouwer et al., 2020; Cao et al., 2020; Chen et al., 2020; Chi et al., 2020; Ju et al., 2020; Liu et al., 2020b; Pinto et al., 2020; Robbiani et al., 2020; Rogers et al., 2020; Seydoux et al., 2020; Wang et al., 2020a; Wrapp et al., 2020a; Wu et al., 2020b; Zeng et al., 2020; Zost et al., 2020). Structural studies (Barnes et al., 2020a, 2020b; Liu et al., 2020a; Wang et al., 2020b; Yuan et al., 2020) have revealed neutralizing antibodies to recognize RBD at multiple distinct sites, and have further revealed multi-donor



RBD-directed antibody classes that appear to be elicited with high frequency in the human population (Barnes et al., 2020b; Robbiani et al., 2020; Wu et al., 2020a; Yuan et al., 2020). Neutralization for many RBD-directed antibodies can be explained by interference with RBD-ACE2 interaction and/or impeding the ability of RBD to adopt the “up” conformation (Barnes et al., 2020b; Liu et al., 2020a; Yuan et al., 2020) required for ACE2 binding (Benton et al., 2020).

The most effective NTD-directed neutralizing antibodies have potencies rivaling those of the best RBD-directed neutralizing antibodies, and recent studies have extensively characterized the NTD-directed antibody response for SARS-CoV-2. McCallum et al. (2021b) isolated a panel of 41 NTD-directed antibodies and mapped their recognition to three sites. Remarkably, all of the antibodies with neutralizing activity mapped to a single site, site 1. In a parallel study, we determined the structures for seven NTD-directed antibodies selected for their potent neutralizing activities, finding them all to target a single supersite (Cerutti et al., 2021a) that coincides with site 1, identified by McCallum et al. Both papers designated the site 1 region as an “antigenic supersite,” targeted by diverse lineages of neutralizing antibodies. In addition to these studies, Suryadevara et al. (2021) determined structures of two NTD-directed neutralizing antibodies, both of which targeted the site 1 supersite. Four additional cryo-electron microscopy (cryo-EM) structures for SARS-CoV-2 NTD-directed neutralizing antibodies—4A8, FC05, CM25, and DH1050.1—reveal binding to the site 1 antigenic supersite (Chi et al., 2020; Li et al., 2021; Voss et al., 2021; Wang et al., 2021a), while a single structure for a non-neutralizing antibody, DH1052, shows targeting outside the supersite (Li et al., 2021). Overall, these results supported the idea that the site 1 supersite represented the lone site of neutralization vulnerability in NTD, which results in high selection pressure for viral escape.

Structural studies have characterized the NTD antigenic supersite and other non-neutralizing epitopes on NTD (Figure S1). NTD is highly glycosylated, and the site 1 supersite, located at the periphery of the spike, is the largest glycan-free surface on NTD facing away from the viral membrane (Cerutti et al., 2021a). Antibodies bind to a region of flexible loops, centered on the N3 β hairpin. The supersite is highly electro-positive. Epitopes to other less potent or non-neutralizing antibodies have also been mapped and numbered as sites 2–6. The basis for the restriction of potent neutralization to site 1 is unclear; however, preliminary studies are consistent with a conformational mechanism for supersite-directed antibodies in which membrane fusion is inhibited (McCallum et al., 2021b; Suryadevara et al., 2021). Despite the potent neutralization of the initial 2019 strain of SARS-CoV-2 achieved by neutralizing antibodies, numerous VOCs have emerged, some of which show concerning resistance to neutralizing antibodies. Antibodies that target the NTD antigenic supersite appear to be particularly vulnerable to escape, with many losing all activity against the alpha, beta, and gamma VOCs (Wang et al., 2021b; Wang et al., 2021c).

The NTD-recognizing antibody 5-7 was isolated from a convalescent donor with severe acute symptoms, displaying a very robust plasma neutralization response, as described in our pre-

vious study (Liu et al., 2020a). Here, we describe the cryo-EM structure of antibody 5-7 in complex with SARS-CoV-2 spike, present neutralization data with VOCs, and analyze the recognized epitope. We show that the 5-7 binding site represents a second site of neutralization vulnerability in SARS-CoV-2 NTD remote from most VOC mutations, underscoring the potential therapeutic value of antibody 5-7.

RESULTS

Antibody 5-7 targets a hydrophobic pocket in NTD

From a complex of SARS-CoV-2 spike—stabilized by 2P mutations (Wrapp et al., 2020b)—with the antigen-binding fragment (Fab) of antibody 5-7, we collected single-particle data on a Titan Krios microscope, yielding a cryo-EM reconstruction to an overall resolution of 3.5 Å for the global refinement and 3.8 Å for the local refinement of the 5-7:NTD interface (Figures 1A and S1–S4; Table S1). The major 3-dimensional (3D) class was C3 symmetrical, with 3 Fabs per trimer. Recognition of NTD by 5-7 was dominated by the heavy chain, which buried a 1,074.2-Å² surface area, with a smaller 146.2-Å² contribution by the light chain. The 24-amino acid complementarity determining region (CDR) H3 formed the dominant interaction with NTD, with additional contributions from CDRs H1, H2, L1, and L3 (Figures 1B and S4A). CDR H3 formed hydrophobic and hydrogen bond contacts with NTD, in particular through residues near the tip of the CDR H3 loop, W100f, S100h, L100i, and K100j, which are within a short helix. Further toward the base of CDR H3, two hydrogen bonds are formed with NTD and additional hydrophobic contacts are formed, particularly with the side chain of CDR H3 Y100e. CDR H1 and H2 contributed to NTD recognition mainly through hydrogen bonds involving N52 and S56 and hydrophobic contacts involving Y33 and V50. Light chain interacted with NTD residues Q173 and P174 through the hydrogen bond and hydrophobic interactions, respectively (Figure S4A).

Antibody 5-7 targets a site distinct from the NTD supersite

Since other neutralizing antibodies targeting NTD recognize the site 1 antigenic supersite, we compared the recognition of NTD by 5-7 and other neutralizing antibodies, most of which are supersite antibodies. We produced a structural superposition of all NTD-directed antibodies deposited in the PDB, superposed on NTD C α atoms, in the context of SARS-CoV-2 spike trimer (Figure 2A). All neutralizing antibodies target the NTD supersite, except for 5-7 and P008_056; these two antibodies bind to different regions on the “side” of NTD. The single non-neutralizing antibody DH1052 binds to another region at the “bottom” of NTD.

Overall, the 5-7 recognition site and NTD supersite (as defined by Cerutti et al., 2021a) are distinct, with a small area of overlap. This can be seen in the ribbon diagram in Figure 2B comparing the NTD supersite shown in magenta with the 5-7 epitope shown in blue. The overlap region only includes 3 residues (150–152) located in the N3 loop. Since the supersite was defined for multiple antibodies of different classes, it is larger than the footprint of any single supersite antibody. Nevertheless, of the

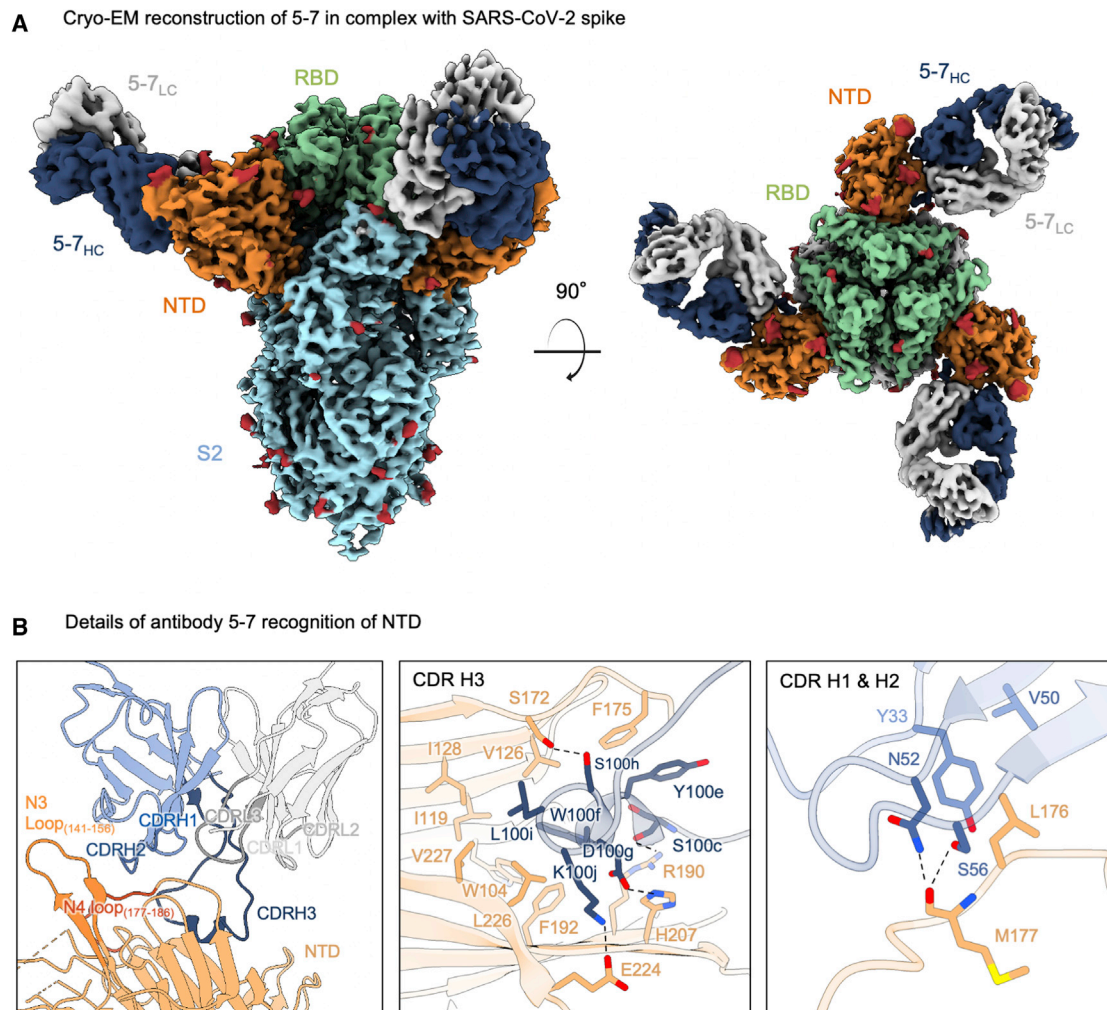


Figure 1. Antibody 5-7 targets a hydrophobic pocket in NTD

(A) Cryo-EM reconstruction for spike complex with antibody 5-7 from 2 orthogonal views. The map shown is a composite map obtained combining the overall map (3.50 Å resolution) and the locally refined map for the 5-7:NTD interface (3.82 Å resolution). NTD is shown in orange, RBD in green, glycans in red, antibody heavy chain in blue, and light chain in gray.

(B) Details of antibody 5-7 recognition of NTD showing the overall interface (left), recognition by CDR H3 (center), and recognition by CDR H1 and H2 (right). CDR H1, H2, and H3 are colored in shades of blue; CDR L1, L2, and L3 are colored in shades of gray. Nitrogen atoms are colored in blue, oxygen atoms in red, and hydrogen bonds (distance <3.2 Å) are represented as dashed lines.

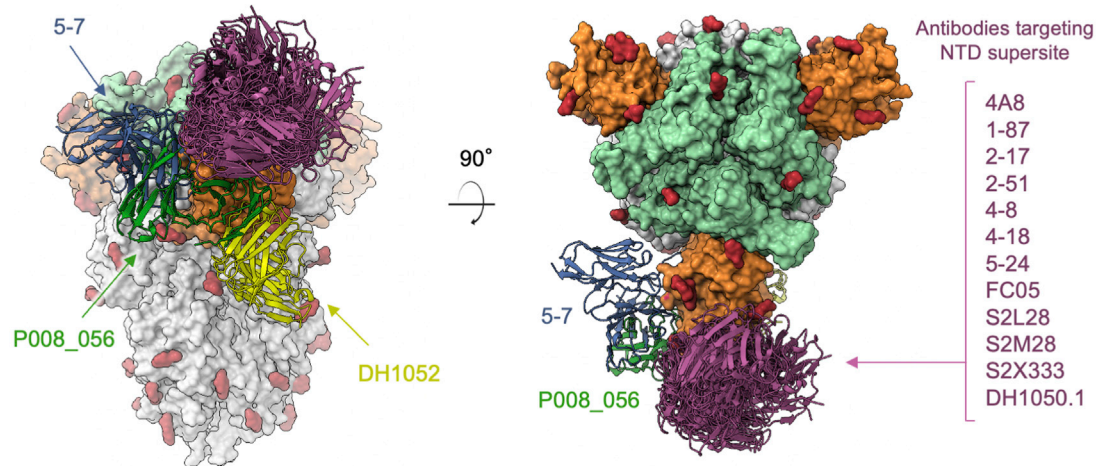
See also [Figures S1–S4](#) and [Table S1](#).

12 supersite antibodies we assessed, all of them, except S2L28, show direct van der Waals clashes with 5-7, localized either to the N3 β harpin or in the N4 loop region.

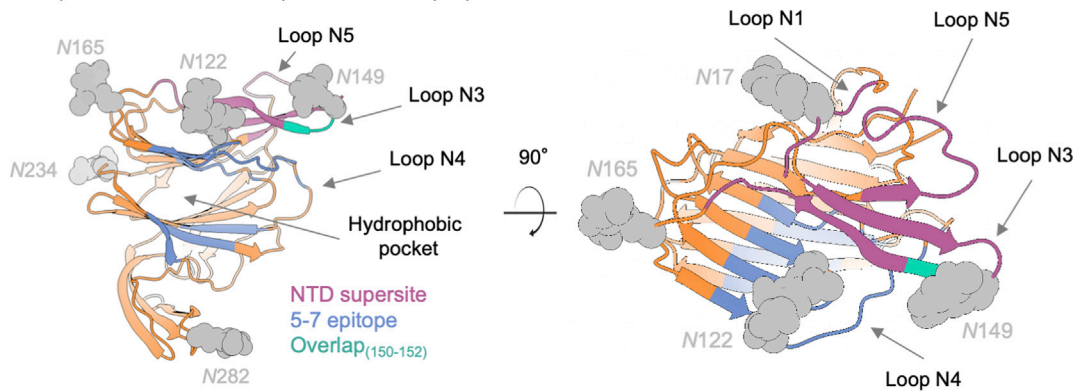
The hydrophobic pocket that accommodates 5-7 CDR H3 has been previously reported to bind hydrophobic ligands, including polysorbate 80 (Bangaru et al., 2020) and biliverdin (Rosa et al., 2021). Comparison of the structure of NTD in complex with polysorbate 80 with the structure of the 5-7 NTD complex revealed nearly identical recognition within the hydrophobic pocket (Figure 2C). It has been suggested that such ligands could prevent the binding of supersite antibodies by conformational competition (Rosa et al., 2021). We therefore assessed the binding of 5-7 and supersite antibodies 4-8 and 5-24 to NTD in the pres-

ence of these small molecules (Figure S6). We ran surface plasmon resonance (SPR) binding experiments in the presence of biliverdin, bilirubin, and polysorbate 80, all reported to bind to the 5-7 pocket, with each at a concentration greater than natural abundance (Shum et al., 2021) and >10-fold its K_D for binding NTD. In each case, binding was observed, despite attenuated affinity in the case of biliverdin for 5-7 binding NTD. Consistently, pseudovirus neutralization experiments showed that the potency of 5-7 is attenuated marginally (~4-fold) after the addition of 10 mM biliverdin, indicating that heme metabolites may not prevent virus neutralization by 5-7 (Figure S7A). In contrast, we observed that the neutralization potency of the NTD supersite antibodies 5-24 and 4-8 were attenuated ~200-fold by biliverdin

A Structural superposition of NTD-directed antibodies on NTD



B Comparison between NTD supersite and 5-7 epitope



C Comparison between NTD in complex with 5-7 and NTD bound to polysorbate 80

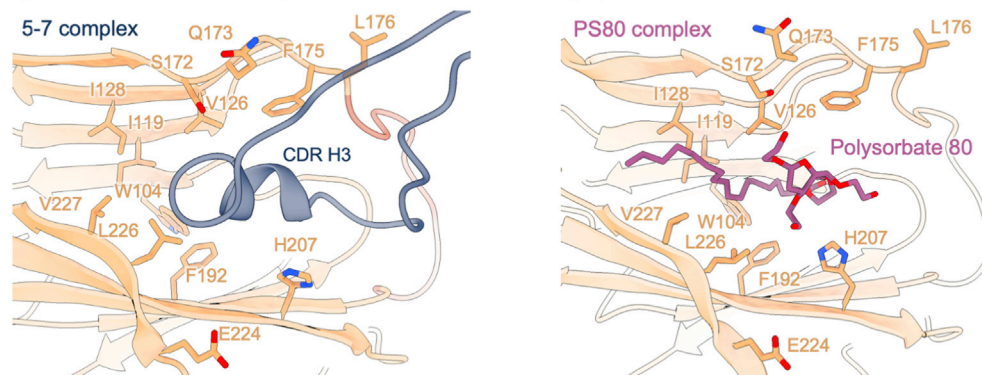


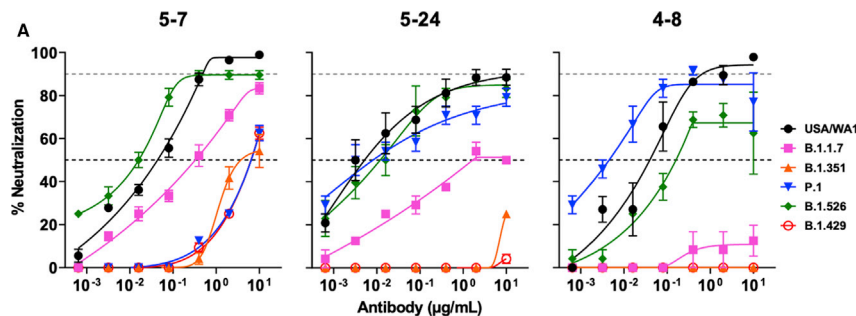
Figure 2. Antibody 5-7 adopts a different binding mode compared to antibodies targeting the NTD supersite

(A) Structural superposition of all NTD-directed antibodies deposited in the PDB on NTD in the context of SARS-CoV-2 spike trimer. All neutralizing antibodies target the NTD supersite (magenta) except for 5-7 (blue) and P008_056 (green). The non-neutralizing antibody DH1052 (yellow) binds to a different region at the “bottom” of NTD.

(B) Comparison between NTD supersite (magenta) and 5-7 epitope (blue) on NTD. The overlap region only includes 3 residues (150–152) located in the N3 loop.

(C) The hydrophobic pocket that accommodates 5-7 CDR H3 (left) has been previously reported to bind polysorbate 80 (right).

See also [Figures S1, S4, S6, and S7](#).



B

| Fold change in IC ₅₀ from WT | 5-7 | 5-24 | 4-8 |
|---|--------|--------|--------|
| B.1.1.7 | -11.9 | <-1000 | <-1000 |
| 69-70del | -4.0 | 1.1 | 1.1 |
| 144del | -3.7 | <-1000 | <-1000 |
| B.1.351 | -18.1 | <-1000 | <-1000 |
| L18F | -8.9 | -2.2 | 1.3 |
| D80A | -9.8 | 2.3 | 2.0 |
| D215G | 1.1 | -1.1 | -1.8 |
| 242-244del | -20.7 | <-1000 | <-1000 |
| R246I | -9.2 | <-1000 | <-1000 |
| P.1 | <-1000 | -1.3 | 6.6 |
| L18F | -9.1 | -1.3 | 2.5 |
| T20N | -4.1 | -1.7 | -1.1 |
| P26S | -1.6 | -3.2 | 1.5 |
| D138Y | -5.5 | -1.1 | 5.1 |
| R190S | -6.1 | 1.5 | 1.0 |
| B.1.526 | -15.2 | -36.7 | -204.5 |
| L5F | -1.5 | 2.5 | -1.6 |
| T95I | -3.9 | 6.7 | -1.3 |
| D253G | -2.8 | -2.8 | <-1000 |
| B.1.427/9 | <-1000 | <-1000 | <-1000 |
| S13I | -34.7 | <-1000 | <-1000 |
| W152C | -18.9 | <-1000 | -296.4 |

(Figure S7A), although the NTD binding affinity of both antibodies was not affected (Figure S6).

Neutralization by antibody 5-7 is partially tolerant to B.1.1.7, B.1.351, and B.1.526 variants

We assessed the neutralization of 5 variants of SARS-CoV-2 infectious virus using 3 antibodies directed against NTD (5-7, 5-24, and 4-8) and 1 directed against RBD (2-7) as a negative control (Figures 3A and S5A). While the potency of all of the NTD monoclonal antibodies (mAbs) was lowered against the variants in comparison to the original isolate (WA1), we found that only one of the mAbs, 5-7, retained ~50% of the neutralization activity to all of the examined variants. This difference in functional behavior of 5-7 against the live viruses was dissected by generating the key NTD mutations into vesicular stomatitis virus (VSV)-

Figure 3. SARS-CoV-2 neutralization profiles for 5-7 and two NTD supersite targeting antibodies

(A) Neutralization of wild-type (USA/WA1), B.1.1.7, B.1.351, P.1, B.1.526, and B.1.429 authentic viruses by NTD-directed mAbs 5-7, 5-24, and 4-8. The horizontal dotted lines on each graph indicate 50% and 90% neutralization. Data are means ± SEMs of technical triplicates and represent 1 of 2 independent experiments.

(B) Fold increase or decrease in IC₅₀ of the mAbs against pseudoviruses containing all of the combined mutations or the NTD single mutation of B.1.1.7, B.1.351, P.1, B.1.526, and B.1.427/9, relative to the wild-type (D614G) virus, presented as a heatmap in which darker colors indicate a greater change. Red, resistance >5-fold; green, sensitization > 5-fold.

See also Figures S5 and S7.

based pseudovirus followed by testing the neutralization of each virus. Antibody 5-7 showed very different neutralization profiles as compared to the 2 NTD supersite targeting antibodies, 5-24 and 4-8. While 5-24 and 4-8 completely lost their activities against the mutations in the NTD supersite (144del, W152C, 242-244del, and R246I), 5-7 still retained its activity, at least partially, against those mutations (Figures 3B and S5B).

The epitope of antibody 5-7 is remote from most VOC mutations

While potency was reduced, antibody 5-7 retained ~50% neutralization activity to all of the variants examined as live virus. To understand the basis for this tolerance, we mapped the mutations of each variant, alpha (B.1.1.7), beta (B.1.351), gamma (P.1), epsilon (B.1.427/9), and iota (B.1.526), to the surface of NTD in the spike complex structure with the 5-7

we report here (Figure 4A). Of the 17 mutations, L5F and S13I located within the signal peptide, 8 mapped within the footprint of the supersite. The epitope of antibody 5-7 contains 2 VOC mutants, R190S in the gamma P.1 virus and W152C in the epsilon B.1.427/9 variant. The structure modeling reveals that both R190S and W152C impair 5-7 binding by altering the local conformation of NTD loops (Figure S4B). R190S and W152C each attenuates pseudovirus half-maximal inhibitory concentration (IC₅₀) by 6.1- and 18.9-fold, respectively. We also observed that NTD mutations far from the 5-7 epitope attenuate 5-7 potency (Figure 3B), suggesting that other mutations may remotely modulate the conformation of NTD, a mechanism similar to other NTD-directed antibodies (McCallum et al., 2021a; Wang et al., 2021b). This agrees with the more substantial attenuation of

5-7 potency observed with live virus neutralization for the P.1 and B.1.427/9 strains (Figure 3A).

To assess the potential breadth of 5-7, we compared the sequence entropy of its epitope among SARS-CoV-2 sequences in the GISAID database to the sequence entropy of the supersite targeted by neutralizing antibodies, and the rest of the NTD surface (Figure 4B). The sequence entropy of the 5-7 epitope is ~1 order of magnitude lower than that of the supersite. Not surprisingly, the W152 and R190 showed the highest entropy within the 5-7 interface; the other residues are highly conserved. Overall, this shows that the 5-7 epitope has low variability and suggests that 5-7 can successfully target numerous circulating SARS-CoV-2 variants.

DISCUSSION

The structure of 5-7 in complex with SARS-CoV-2 spike shows that potent neutralization can be achieved by antibodies that target NTD outside of the site 1 supersite. *In vitro* experiments suggest that supersite-directed antibodies neutralize not by blocking recognition of the ACE2 receptor but by inhibiting conformational changes required for fusion (Suryadevara et al., 2021). It is possible that 5-7, which binds at a site near to but distinct from the supersite and also fails to inhibit interaction with ACE2 (Liu et al., 2020a), could function through a similar mechanism.

Despite the clear structural uniqueness of antibody 5-7, prior experiments showed binding competition between 5-7 and supersite-directed antibodies (Liu et al., 2020a). The strong competition observed between 5-7 and all supersite antibodies could be steric, but could also involve conformational competition: comparison of the NTD conformations observed in each antibody revealed a structural coupling between the N3 β harpin and the N4 loop outlining the epitope of 5-7, which acts as a gate for the hydrophobic pocket (Figure S4C). In most antibody-bound structures, the N4 loop adopts a “closed” conformation, preventing exposure of the hydrophobic pocket, but the “open” conformation is required to accommodate the CDR H3 loop of 5-7. The N4 loop in the S2L28-bound NTD structure was modeled in the “open” conformation, thus resembling the conformation observed in the structure of 5-7-bound NTD, but the EM density shows an equilibrium of both “open” and “closed” states. As a result, the NTD conformation observed in the 5-7 complex structure is unique and appears to be incompatible with the binding of other reported NTD-directed neutralizing antibodies. The only exception was neutralizing antibody PVI.V6-14, reported at the time of the submission of this paper, which shows a binding mode similar to 5-7 (Altomare et al., 2021).

The site that accommodates CDR H3, between the two sheets of the NTD β sandwich, has also been shown to accommodate small-molecule ligands, including a detergent, polysorbate 80 (Bangaru et al., 2020), and heme metabolites biliverdin and bilirubin (Rosa et al., 2021). The SPR binding experiments reported here show that binding these compounds does not significantly interfere with recognition by 5-7 or supersite antibodies 5-24 and 4-8 (Figure S6). The pseudovirus neutralization showed that the potency of 5-7 does not decrease much

(~4-fold) with the addition of biliverdin. However, the potency of antibodies 5-24 and 4-8 are significantly decreased by biliverdin (Figure S7A), which is consistent with a previous study on other NTD-directed antibodies, including an antibody, P008_056, that recognizes an epitope that overlaps significantly with 5-7 (Rosa et al., 2021). The different impacts of biliverdin on these NTD-directed antibodies imply that 5-7 may neutralize SARS-CoV-2 with a mechanism different from many other NTD-directed neutralizing antibodies. Our structural analysis further revealed that antibody 5-7 competes with biliverdin differently from P008_056. Antibody 5-7 inserts its CDR H3 directly to the binding pocket of biliverdin for competition, whereas P008_056 competes with biliverdin by binding to the N4 loop to alter the conformation of the biliverdin binding pocket (Figure S7B). This hydrophobic pocket may play a role in SARS-CoV-2 biology, such as interacting with a target protein ligand, but if so, this remains unknown. The binding of biliverdin and bilirubin has been proposed as a means of viral evasion (Rosa et al., 2021), although we find here that the immune system is able to generate an antibody that turns this binding pocket into a site of vulnerability for antibody neutralization.

Among the more attractive properties of antibody 5-7 is the partial tolerance of its neutralization to VOC mutations. We have shown here that this tolerance arises largely due to its novel binding orientation, which leads to a lack of overlap of 5-7 with VOC mutations. Overall, we have shown 5-7 to target a conserved epitope on NTD, increasing the number of known neutralizing epitopes and enabling therapeutic strategies such as cocktail combinations or multi-specifics that target both NTD and RBD.

Limitations of the study

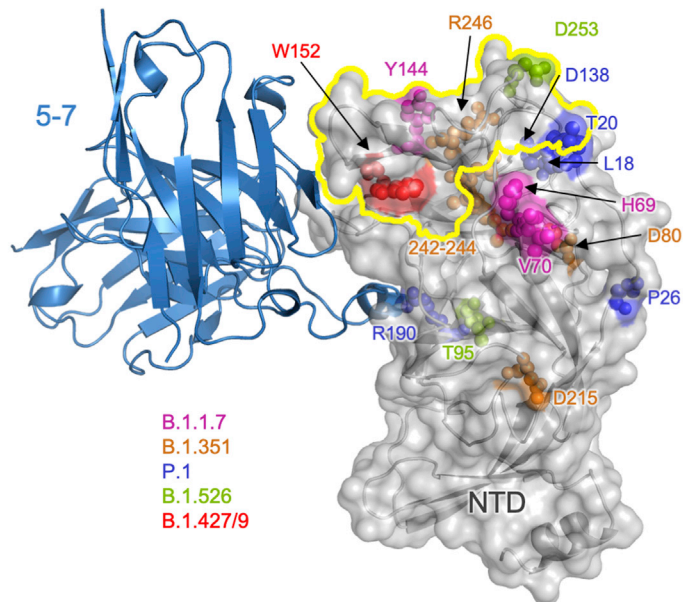
The cryo-EM reconstruction reported in this article was suboptimal in the constant region of the Fab, probably due to flexibility with respect to the Fv region; deposited coordinates do not include modeling of the CH1 and CL1 domains. Because of the intrinsic flexibility of certain regions of spike, the EM map did not allow modeling of the following regions: the N2 and N5 loops of NTD, the S1/S2 cleavage site, the switch region, and the C terminus (residues >1,145). A few residues in the SD1 domain of spike were modeled as stubs (Ala) since side chains were not visible in the EM map. Finally, SARS-CoV-2 neutralization by antibody 5-7 was not tested against the delta (B.1.617.2), kappa (B.1.617.1), mu (B.1.621), and zeta (P.2) VOCs.

STAR★METHODS

Detailed methods are provided in the online version of this paper and include the following:

- KEY RESOURCES TABLE
- RESOURCE AVAILABILITY
 - Lead contact
 - Materials availability
 - Data and code availability
- EXPERIMENTAL MODEL AND SUBJECT DETAILS
 - Cell lines

A NTD mutations in emerging SARS-CoV-2 variants



B

Entropy of residues in 5-7 epitope and NTD supersite

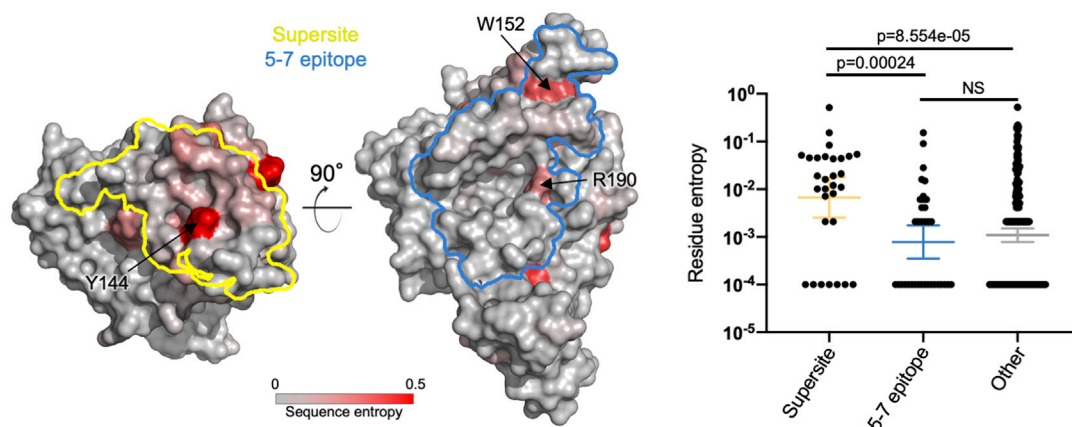


Figure 4. Antibody 5-7 binds apart from most of the mutations in emerging SARS-CoV-2 variants

(A) The majority of NTD mutations in different SARS-CoV-2 variants are not within the 5-7 binding region. Mutations in B.1.1.7 are colored magenta, B.1.351 orange, P.1 blue, B.1.526 green, and B.1.427/9 red. The NTD supersite is outlined in yellow.

(B) Comparison of residue entropy between NTD supersite, 5-7 epitope, and other residues on NTD. Larger entropy means more diversification. Left and center panels show the footprint and residue entropy for the supersite and 5-7 epitope on the NTD surface. Right: residues are represented as dots, and the geometric mean and 95% confidence interval (CI) of the 3 groups of residues are shown in blue, red, and green, respectively. Antibody 5-7 epitope residues are the most conserved among the 3 groups. The p values between different groups were calculated using the Kolmogorov-Smirnov test.

See also [Figure S4](#).

● **METHOD DETAILS**

- Protein samples expression and purification
- Cryo-EM sample preparation
- Cryo-EM data collection, processing and structure refinement
- Authentic SARS-CoV-2 microplate neutralization

- Pseudovirus neutralization assays
- Biliverdin pseudovirus neutralization assays
- SPR experiments
- Antibody gene assignments and genetic analyses
- Sequence entropy comparison

● **QUANTIFICATION AND STATISTICAL ANALYSIS**

SUPPLEMENTAL INFORMATION

Supplemental information can be found online at <https://doi.org/10.1016/j.celrep.2021.109928>.

ACKNOWLEDGMENTS

We thank R. Grassucci, Y.-C. Chi, and Z. Zhang from the Cryo-EM Center at Columbia University for assistance with cryo-EM data collection. Support for this work was also provided by the Intramural Program of the Vaccine Research Center, National Institutes of Allergy and Infectious Diseases, NIH, and by Samuel Yin, Pony Ma, Peggy & Andrew Cherng, Bria Biosciences, the Jack Ma Foundation, the JBP Foundation, Carol Ludwig, Roger & David Wu, COVID-19 Fast Grants, the Self Graduate Fellowship Program, and NIH grants DP5OD023118, R21AI143407, and R21AI144408.

AUTHOR CONTRIBUTIONS

G.C. determined the cryo-EM structure of 5-7, Y.G. performed the bioinformatics analysis. P.W., M.S.N., M.W., Y.H., J.Y., L.L., and D.D.H. contributed data on neutralization assays and also produced immunoglobulin Gs (IgGs) and Fabs. F.B. produced spike. J.Y. and E.R.R. produced Fabs. D.D.H. supervised IgG production and the neutralization assay. P.D.K. contributed to the bioinformatics and structural analysis. Z.S. supervised the bioinformatics analysis. L.S. supervised the structural determinations and led the overall project. G.C., Y.G., P.D.K., Z.S., and L.S. wrote the manuscript, with all of the authors' comments.

DECLARATION OF INTERESTS

D.D.H., Y.H., J.Y., L.L., and P.W. are inventors of a patent describing some of the antibodies reported here.

Received: June 10, 2021

Revised: August 27, 2021

Accepted: October 12, 2021

Published: October 16, 2021

REFERENCES

- Adams, P.D., Gopal, K., Grosse-Kunstleve, R.W., Hung, L.W., Ioerger, T.R., McCoy, A.J., Moriarty, N.W., Pai, R.K., Read, R.J., Romo, T.D., et al. (2004). Recent developments in the PHENIX software for automated crystallographic structure determination. *J. Synchrotron Radiat.* *11*, 53–55.
- Altomare, C.G., Adelsberg, D.C., Carreno, J.M., Sapse, I.A., Amanat, F., Ellebedy, A.H., Simon, V., Krammer, F., and Bajic, G. (2021). Structure of a germ-line-like human antibody defines a neutralizing epitope on the SARS-CoV-2 spike NTD. *bioRxiv*. <https://doi.org/10.1101/2021.07.08.451649>.
- Annavajhala, M.K., Mohri, H., Zucker, J.E., Sheng, Z., Wang, P., Gomez-Simmonds, A., Ho, D.D., and Uhlemann, A.C. (2021). A Novel SARS-CoV-2 Variant of Concern, B.1.526, Identified in New York. *medRxiv*. <https://doi.org/10.1101/2021.02.23.21252259>.
- Bangaru, S., Ozorowski, G., Turner, H.L., Antanasijevic, A., Huang, D., Wang, X., Torres, J.L., Diedrich, J.K., Tian, J.H., Portnoff, A.D., et al. (2020). Structural analysis of full-length SARS-CoV-2 spike protein from an advanced vaccine candidate. *Science* *370*, 1089–1094.
- Barad, B.A., Echols, N., Wang, R.Y., Cheng, Y., DiMaio, F., Adams, P.D., and Fraser, J.S. (2015). EMRinger: side chain-directed model and map validation for 3D cryo-electron microscopy. *Nat. Methods* *12*, 943–946.
- Barnes, C.O., Jette, C.A., Abernathy, M.E., Dam, K.A., Esswein, S.R., Gristick, H.B., Malyutin, A.G., Sharaf, N.G., Huey-Tubman, K.E., Lee, Y.E., et al. (2020a). SARS-CoV-2 neutralizing antibody structures inform therapeutic strategies. *Nature* *588*, 682–687.
- Barnes, C.O., West, A.P., Jr., Huey-Tubman, K.E., Hoffmann, M.A.G., Sharaf, N.G., Hoffman, P.R., Koranda, N., Gristick, H.B., Gaebler, C., Muecksch, F., et al. (2020b). Structures of Human Antibodies Bound to SARS-CoV-2 Spike Reveal Common Epitopes and Recurrent Features of Antibodies. *Cell* *182*, 828–842.e16.
- Benton, D.J., Wrobel, A.G., Xu, P., Roustan, C., Martin, S.R., Rosenthal, P.B., Skehel, J.J., and Gamblin, S.J. (2020). Receptor binding and priming of the spike protein of SARS-CoV-2 for membrane fusion. *Nature* *588*, 327–330.
- Bepler, T., Morin, A., Rapp, M., Brasch, J., Shapiro, L., Noble, A.J., and Berger, B. (2019). Positive-unlabeled convolutional neural networks for particle picking in cryo-electron micrographs. *Nat. Methods* *16*, 1153–1160.
- Brochet, X., Lefranc, M.-P., and Giudicelli, V. (2008). IMGT/V-QUEST: the highly customized and integrated system for IG and TR standardized V-J and V-D-J sequence analysis. *Nucleic Acids Res.* *36*, W503–W508.
- Brouwer, P.J.M., Caniels, T.G., van der Straten, K., Snitselaar, J.L., Aldon, Y., Bangaru, S., Torres, J.L., Okba, N.M.A., Claireaux, M., Kerster, G., et al. (2020). Potent neutralizing antibodies from COVID-19 patients define multiple targets of vulnerability. *Science* *369*, 643–650.
- Callaway, E., Cyranoski, D., Mallapaty, S., Stoye, E., and Tollefson, J. (2020). The coronavirus pandemic in five powerful charts. *Nature* *579*, 482–483.
- Cao, Y., Su, B., Guo, X., Sun, W., Deng, Y., Bao, L., Zhu, Q., Zhang, X., Zheng, Y., Geng, C., et al. (2020). Potent neutralizing antibodies against SARS-CoV-2 identified by high-throughput single-cell sequencing of convalescent patients' B cells. *Cell* *182*, 73–84.e16.
- Cerutti, G., Guo, Y., Zhou, T., Gorman, J., Lee, M., Rapp, M., Reddem, E.R., Yu, J., Bahna, F., Bimela, J., et al. (2021a). Potent SARS-CoV-2 neutralizing antibodies directed against spike N-terminal domain target a single supersite. *Cell Host Microbe* *29*, 819–833.e7.
- Cerutti, G., Rapp, M., Guo, Y., Bahna, F., Bimela, J., Reddem, E.R., Yu, J., Wang, P., Liu, L., Huang, Y., et al. (2021b). Structural basis for accommodation of emerging B.1.351 and B.1.1.7 variants by two potent SARS-CoV-2 neutralizing antibodies. *Structure* *29*, 1–9.
- Chen, X., Li, R., Pan, Z., Qian, C., Yang, Y., You, R., Zhao, J., Liu, P., Gao, L., Li, Z., et al. (2020). Human monoclonal antibodies block the binding of SARS-CoV-2 spike protein to angiotensin converting enzyme 2 receptor. *Cell. Mol. Immunol.* *17*, 647–649.
- Chi, X., Yan, R., Zhang, J., Zhang, G., Zhang, Y., Hao, M., Zhang, Z., Fan, P., Dong, Y., Yang, Y., et al. (2020). A neutralizing human antibody binds to the N-terminal domain of the Spike protein of SARS-CoV-2. *Science* *369*, 650–655.
- Cucinotta, D., and Vanelli, M. (2020). WHO Declares COVID-19 a Pandemic. *Acta Biomed.* *91*, 157–160.
- Davis, I.W., Murray, L.W., Richardson, J.S., and Richardson, D.C. (2004). MOLPROBITY: structure validation and all-atom contact analysis for nucleic acids and their complexes. *Nucleic Acids Res.* *32*, W615–W619.
- Dong, E., Du, H., and Gardner, L. (2020). An interactive web-based dashboard to track COVID-19 in real time. *Lancet Infect. Dis.* *20*, 533–534.
- Dunbar, J., Krawczyk, K., Leem, J., Marks, C., Nowak, J., Regep, C., Georges, G., Kelm, S., Popovic, B., and Deane, C.M. (2016). SAbPred: a structure-based antibody prediction server. *Nucleic Acids Res.* *44* (W1), W474–W478.
- Emsley, P., and Cowtan, K. (2004). Coot: model-building tools for molecular graphics. *Acta Crystallogr. D Biol. Crystallogr.* *60*, 2126–2132.
- Grant, B.J., Rodrigues, A.P., ElSawy, K.M., McCammon, J.A., and Caves, L.S. (2006). Bio3d: an R package for the comparative analysis of protein structures. *Bioinformatics* *22*, 2695–2696.
- Guo, Y., Chen, K., Kwong, P.D., Shapiro, L., and Sheng, Z. (2019). cAb-Rep: A Database of Curated Antibody Repertoires for Exploring Antibody Diversity and Predicting Antibody Prevalence. *Front. Immunol.* *10*, 2365.
- Hadfield, J., Megill, C., Bell, S.M., Huddleston, J., Potter, B., Callender, C., Sargulenko, P., Bedford, T., and Neher, R.A. (2018). Nextstrain: real-time tracking of pathogen evolution. *Bioinformatics* *34*, 4121–4123.
- Ju, B., Zhang, Q., Ge, J., Wang, R., Sun, J., Ge, X., Yu, J., Shan, S., Zhou, B., Song, S., et al. (2020). Human neutralizing antibodies elicited by SARS-CoV-2 infection. *Nature* *584*, 115–119.

- Krissinel, E., and Henrick, K. (2007). Inference of macromolecular assemblies from crystalline state. *J. Mol. Biol.* *372*, 774–797.
- Li, D., Edwards, R.J., Manne, K., Martinez, D.R., Schäfer, A., Alam, S.M., Wiehe, K., Lu, X., Parks, R., Sutherland, L.L., et al. (2021). The functions of SARS-CoV-2 neutralizing and infection-enhancing antibodies in vitro and in mice and nonhuman primates. *bioRxiv*. <https://doi.org/10.1101/2020.2012.2031.424729>.
- Liu, L., Wang, P., Nair, M.S., Yu, J., Rapp, M., Wang, Q., Luo, Y., Chan, J.F., Sahi, V., Figueroa, A., et al. (2020a). Potent neutralizing antibodies against multiple epitopes on SARS-CoV-2 spike. *Nature* *584*, 450–456.
- Liu, X., Gao, F., Gou, L., Chen, Y., Gu, Y., Ao, L., Shen, H., Hu, Z., Guo, X., and Gao, W. (2020b). Neutralizing Antibodies Isolated by a Site-directed Screening have Potent Protection on SARS-CoV-2 Infection. *bioRxiv*. <https://doi.org/10.1101/2020.2005.2003.074914>.
- McCallum, M., Bassi, J., Marco, A., Chen, A., Walls, A.C., Iulio, J.D., Tortorici, M.A., Navarro, M.J., Silacci-Fregni, C., Saliba, C., et al. (2021a). SARS-CoV-2 immune evasion by variant B.1.427/B.1.429. *bioRxiv*. <https://doi.org/10.1101/2021.03.31.437925>.
- McCallum, M., De Marco, A., Lempp, F.A., Tortorici, M.A., Pinto, D., Walls, A.C., Beltramello, M., Chen, A., Liu, Z., Zatta, F., et al. (2021b). N-terminal domain antigenic mapping reveals a site of vulnerability for SARS-CoV-2. *Cell* *184*, 2332–2347.e16.
- Faria, N.R., Morales Claro, I., Candido, D., Moyses Franco, L.A., Andrade, P.S., Coletti, T.M., Silva, C.A.M., Sales, F.C., Manuli, E.R., Aguiar, R.S., et al. (2021). Genomic characterisation of an emergent SARS-CoV-2 lineage in Manaus: preliminary findings. <https://virological.org/t/genomic-characterisation-of-an-emergent-sars-cov-2-lineage-in-manauas-preliminary-findings/586>.
- Pettersen, E.F., Goddard, T.D., Huang, C.C., Couch, G.S., Greenblatt, D.M., Meng, E.C., and Ferrin, T.E. (2004). UCSF Chimera—a visualization system for exploratory research and analysis. *J. Comput. Chem.* *25*, 1605–1612.
- Pettersen, E.F., Goddard, T.D., Huang, C.C., Meng, E.C., Couch, G.S., Croll, T.I., Morris, J.H., and Ferrin, T.E. (2021). UCSF ChimeraX: structure visualization for researchers, educators, and developers. *Protein Sci.* *30*, 70–82.
- Pinto, D., Park, Y.-J., Beltramello, M., Walls, A.C., Tortorici, M.A., Bianchi, S., Jaconi, S., Culap, K., Zatta, F., De Marco, A., et al. (2020). Structural and functional analysis of a potent sarbecovirus neutralizing antibody. *bioRxiv*. <https://doi.org/10.1101/2020.2004.2007.023903>.
- Punjani, A., Rubinstein, J.L., Fleet, D.J., and Brubaker, M.A. (2017). cryo-SPARC: algorithms for rapid unsupervised cryo-EM structure determination. *Nat. Methods* *14*, 290–296.
- Rapp, M., Guo, Y., Reddem, E.R., Liu, L., Wang, P., Yu, J., Cerutti, G., Bimela, J., Bahna, F., Mannepalli, S., et al. (2021). Modular basis for potent SARS-CoV-2 neutralization by a prevalent VH1-2-derived antibody class. *Cell Rep.* *35*, 108950.
- Robbiani, D.F., Gaebler, C., Muecksch, F., Lorenzi, J.C.C., Wang, Z., Cho, A., Agudelo, M., Barnes, C.O., Gazumyan, A., Finkin, S., et al. (2020). Convergent antibody responses to SARS-CoV-2 in convalescent individuals. *Nature* *584*, 437–442.
- Rogers, T.F., Zhao, F., Huang, D., Beutler, N., Burns, A., He, W.T., Limbo, O., Smith, C., Song, G., Woehl, J., et al. (2020). Isolation of potent SARS-CoV-2 neutralizing antibodies and protection from disease in a small animal model. *Science* *369*, 956–963.
- Rosa, A., Pye, V.E., Graham, C., Muir, L., Seow, J., Ng, K.W., Cook, N.J., Rees-Spear, C., Parker, E., Dos Santos, M.S., et al. (2021). SARS-CoV-2 can recruit a heme metabolite to evade antibody immunity. *Sci. Adv.* *7*, eabg7607.
- Scheres, S.H. (2012). RELION: implementation of a Bayesian approach to cryo-EM structure determination. *J. Struct. Biol.* *180*, 519–530.
- Seydoux, E., Homad, L.J., MacCamy, A.J., Parks, K.R., Hurlburt, N.K., Jennewein, M.F., Akins, N.R., Stuart, A.B., Wan, Y.H., Feng, J., et al. (2020). Characterization of neutralizing antibodies from a SARS-CoV-2 infected individual. *bioRxiv*. <https://doi.org/10.1101/2020.2005.2012.091298>.
- Shum, M., Shintre, C.A., Althoff, T., Gutierrez, V., Segawa, M., Saxberg, A.D., Martinez, M., Adamson, R., Young, M.R., Faust, B., et al. (2021). ABCB1 exports mitochondrial biliverdin, driving metabolic maladaptation in obesity. *Sci. Transl. Med.* *13*, eabd1869.
- Suloway, C., Pulokas, J., Fellmann, D., Cheng, A., Guerra, F., Quispe, J., Stagg, S., Potter, C.S., and Carragher, B. (2005). Automated molecular microscopy: the new Legimon system. *J. Struct. Biol.* *151*, 41–60.
- Suryadevara, N., Shrihari, S., Gilchuk, P., VanBlargan, L.A., Binshtein, E., Zost, S.J., Nargi, R.S., Sutton, R.E., Winkler, E.S., Chen, E.C., et al. (2021). Neutralizing and protective human monoclonal antibodies recognizing the N-terminal domain of the SARS-CoV-2 spike protein. *Cell* *184*, 2316–2331.e15.
- Tang, J.W., Tambyah, P.A., and Hui, D.S. (2021). Emergence of a new SARS-CoV-2 variant in the UK. *J. Infect.* *82*, e27–e28.
- Tegally, H., Wilkinson, E., Giovanetti, M., Iranzadeh, A., Fonseca, V., Giandhari, J., Doolabh, D., Pillay, S., San, E.J., Msomi, N., et al. (2020). Emergence and rapid spread of a new severe acute respiratory syndrome-related coronavirus 2 (SARS-CoV-2) lineage with multiple spike mutations in South Africa. *medRxiv*. <https://doi.org/10.1101/2020.2012.2021.20248640>.
- Voss, W.N., Hou, Y.J., Johnson, N.V., Delidakis, G., Kim, J.E., Javanmardi, K., Horton, A.P., Bartzoka, F., Paresi, C.J., Tanno, Y., et al. (2021). Prevalent, protective, and convergent IgG recognition of SARS-CoV-2 non-RBD spike epitopes. *Science* *372*, 1108–1112.
- Walls, A.C., Park, Y.J., Tortorici, M.A., Wall, A., McGuire, A.T., and Velesler, D. (2020). Structure, Function, and Antigenicity of the SARS-CoV-2 Spike Glycoprotein. *Cell* *181*, 281–292.e6.
- Wang, C., Li, W., Drabek, D., Okba, N.M.A., van Haperen, R., Osterhaus, A.D.M.E., van Kuppeveld, F.J.M., Haagmans, B.L., Grosveld, F., and Bosch, B.J. (2020a). A human monoclonal antibody blocking SARS-CoV-2 infection. *Nat. Commun.* *11*, 2251.
- Wang, Q., Zhang, Y., Wu, L., Niu, S., Song, C., Zhang, Z., Lu, G., Qiao, C., Hu, Y., Yuen, K.Y., et al. (2020b). Structural and Functional Basis of SARS-CoV-2 Entry by Using Human ACE2. *Cell* *181*, 894–904.e9.
- Wang, N., Sun, Y., Feng, R., Wang, Y., Guo, Y., Zhang, L., Deng, Y.Q., Wang, L., Cui, Z., Cao, L., et al. (2021a). Structure-based development of human antibody cocktails against SARS-CoV-2. *Cell Res.* *31*, 101–103.
- Wang, P., Casner, R.G., Nair, M.S., Wang, M., Yu, J., Cerutti, G., Liu, L., Kwong, P.D., Huang, Y., Shapiro, L., and Ho, D.D. (2021b). Increased resistance of SARS-CoV-2 variant P.1 to antibody neutralization. *Cell Host Microbe* *29*, 747–751.e4.
- Wang, P., Nair, M.S., Liu, L., Iketani, S., Luo, Y., Guo, Y., Wang, M., Yu, J., Zhang, B., Kwong, P.D., et al. (2021c). Antibody resistance of SARS-CoV-2 variants B.1.351 and B.1.1.7. *Nature* *593*, 130–135.
- Wrapp, D., De Vlieger, D., Corbett, K.S., Torres, G.M., Wang, N., Van Breedam, W., Roose, K., van Schie, L., Hoffmann, M., Pöhlmann, S., et al.; VIB-CMB COVID-19 Response Team (2020a). Structural Basis for Potent Neutralization of Betacoronaviruses by Single-Domain Camelid Antibodies. *Cell* *181*, 1004–1015.e15.
- Wrapp, D., Wang, N., Corbett, K.S., Goldsmith, J.A., Hsieh, C.L., Abiona, O., Graham, B.S., and McLellan, J.S. (2020b). Cryo-EM structure of the 2019-nCoV spike in the prefusion conformation. *Science* *367*, 1260–1263.
- Wu, N.C., Yuan, M., Bangaru, S., Huang, D., Zhu, X., Lee, C.-C.D., Turner, H.L., Peng, L., Yang, L., Nemazee, D., et al. (2020a). A natural mutation between SARS-CoV-2 and SARS-CoV determines neutralization by a cross-reactive antibody. *bioRxiv*. <https://doi.org/10.1101/2020.2009.2021.305441>.
- Wu, Y., Wang, F., Shen, C., Peng, W., Li, D., Zhao, C., Li, Z., Li, S., Bi, Y., Yang, Y., et al. (2020b). A noncompeting pair of human neutralizing antibodies block COVID-19 virus binding to its receptor ACE2. *Science* *368*, 1274–1278.
- Yadav, P.D., Sapkal, G.N., Abraham, P., Ella, R., Deshpande, G., Patil, D.Y., Nyayanit, D.A., Gupta, N., Sahay, R.R., Shete, A.M., et al. (2021). Neutralization of variant under investigation B.1.617 with sera of BBV152 vaccinees. *bioRxiv*. <https://doi.org/10.1101/2021.2004.2023.441101>.
- Yan, R., Zhang, Y., Li, Y., Xia, L., Guo, Y., and Zhou, Q. (2020). Structural basis for the recognition of SARS-CoV-2 by full-length human ACE2. *Science* *367*, 1444–1448.

- Ye, J., Ma, N., Madden, T.L., and Ostell, J.M. (2013). IgBLAST: an immunoglobulin variable domain sequence analysis tool. *Nucleic Acids Res.* *41*, W34–W40.
- Yuan, M., Liu, H., Wu, N.C., Lee, C.D., Zhu, X., Zhao, F., Huang, D., Yu, W., Hua, Y., Tien, H., et al. (2020). Structural basis of a shared antibody response to SARS-CoV-2. *Science* *369*, 1119–1123.
- Zeng, X., Li, L., Lin, J., Li, X., Liu, B., Kong, Y., Zeng, S., Du, J., Xiao, H., Zhang, T., et al. (2020). Isolation of a human monoclonal antibody specific for the receptor binding domain of SARS-CoV-2 using a competitive phage biopanning strategy. *Antib. Ther.* *3*, 95–100.
- Zhang, W., Davis, B.D., Chen, S.S., Martinez, J.M.S., Plummer, J.T., and Vail, E. (2021). Emergence of a novel SARS-CoV-2 strain in Southern California, USA. *medRxiv*. <https://doi.org/10.1101/2021.2001.2018.21249786>.
- Zhou, T., Tsybovsky, Y., Gorman, J., Rapp, M., Cerutti, G., Chuang, G.Y., Katsamba, P.S., Sampson, J.M., Schön, A., Bimela, J., et al. (2020). Cryo-EM Structures of SARS-CoV-2 Spike without and with ACE2 Reveal a pH-Dependent Switch to Mediate Endosomal Positioning of Receptor-Binding Domains. *Cell Host Microbe* *28*, 867–879.e5.
- Zivanov, J., Nakane, T., and Scheres, S.H.W. (2019). A Bayesian approach to beam-induced motion correction in cryo-EM single-particle analysis. *IUCrJ* *6*, 5–17.
- Zost, S.J., Gilchuk, P., Chen, R.E., Case, J.B., Reidy, J.X., Trivette, A., Nargi, R.S., Sutton, R.E., Suryadevara, N., Chen, E.C., et al. (2020). Rapid isolation and profiling of a diverse panel of human monoclonal antibodies targeting the SARS-CoV-2 spike protein. *Nat. Med.* *26*, 1422–1427.

STAR★METHODS

KEY RESOURCES TABLE

| REAGENT or RESOURCE | SOURCE | IDENTIFIER |
|---|-------------------------------------|-----------------|
| Antibodies | | |
| 5-7 | Liu et al., 2020a | N/A |
| Bacterial and virus strain | | |
| VSV-G pseudo-typed ΔG-luciferase | Kerafast | Cat# EH1020-PM |
| Chemicals, peptides, and recombinant proteins | | |
| SARS-CoV-2 spike protein | Wrapp et al., 2020b | N/A |
| Polyethylenimine | Polysciences | Cat# 24765-2 |
| Freestyle 293 Expression Media | Thermo Scientific | Cat# 12338-026 |
| Expi293 Expression Media | Thermo Scientific | Cat# A14635 |
| Opti-MEM Reduced Serum Media | Thermo Scientific | Cat# 31985-070 |
| IMAC Sepharose 6 Fast Flow | GE Healthcare | Cat# 17092109 |
| Biotin | Sigma | Cat# B4501 |
| Tris Base | Thermo Scientific | Cat# BP152-5 |
| Sodium Chloride | Thermo Scientific | Cat# S271-10 |
| Imidazole | ACROS | Cat# 301870025 |
| HEPES | Sigma | Cat# H3375 |
| Tween-20 | Sigma | Cat# P7949 |
| Series S SA chip | Cytiva | Cat# BR100531 |
| DMSO | Sigma | Cat# 276855 |
| Biliverdin hydrochloride | Sigma | Cat# 30891 |
| Bilirubin | Sigma | Cat# B4126 |
| Polysorbate 80 | Sigma | Cat# P8074 |
| Critical commercial assays | | |
| FuGENE 6 | Promega | Cat# E2691 |
| Strep-Tactin XT Superflow 50% | Zymo research | Cat# P2004-1-5 |
| Spin Miniprep Kit | QIAGEN | Cat# 27106 |
| Hispeed Plasmid Maxi Kit | QIAGEN | Cat# 12663 |
| HisTrap Fast Flow | GE Healthcare | Cat# 17-0921-09 |
| Ni-NTA Agarose | Thermo Scientific | Cat# R90115 |
| Pierce Fab Preparation Kit | Thermo Scientific | Cat# 44985 |
| Superdex 200 Increase 10/300 GL | Cytiva | Cat# 28990945 |
| Deposited data | | |
| Cryo-EM structure of the SARS-CoV-2 spike glycoprotein bound to Fab 5-7 | This paper | PDB: 7RW2 |
| Cryo-EM map of the SARS-CoV-2 spike glycoprotein bound to Fab 5-7 | This paper | EMDB: EMD-24708 |
| Experimental models: cell lines | | |
| Expi293F Cells | Thermo Scientific | Cat# A14635 |
| FreeStyle 293-F | Thermo Scientific | Cat# R79007 |
| HEK293T/17 | ATCC | Cat# CRL-11268 |
| I1 mouse hybridoma | ATCC | Cat# CRL-2700 |
| Vero E6 | ATCC | Cat# CRL-1586 |

(Continued on next page)

Continued

| REAGENT or RESOURCE | SOURCE | IDENTIFIER |
|--|---|---|
| Recombinant DNA | | |
| pCMV3-SARS-CoV-2-spike | Dr. Peihui Wang, Shandong University, China | N/A |
| pLEXm | Laboratory of Daniel Leahy, Johns Hopkins University, USA | N/A |
| pVRC8400 vector | https://www.addgene.org | Cat# 63160 |
| gWiz-blank | Aldevron | Cat# 5009 |
| Software and algorithms | | |
| Coot | Emsley and Cowtan, 2004 | https://www2.mrc-lmb.cam.ac.uk/personal/pemsley/coot |
| cryoSPARC | Punjani et al., 2017 | https://cryosparc.com |
| Leginon | Suloway et al., 2005 | https://sbgrid.org/software/titles/legion |
| Molprobit | Davis et al., 2004 | http://molprobit.biochem.duke.edu |
| Phenix | Adams et al., 2004 | https://phenix-online.org |
| The PyMOL Molecular Graphics System, Version 2.0 | Schrödinger, LLC | https://pymol.org/2/support.html#page-top |
| RELION | Scheres, 2012 | https://www3.mrc-lmb.cam.ac.uk/relion/index.php/Main_Page |
| SABPred | Dunbar et al., 2016 | http://opig.stats.ox.ac.uk/webapps/newsabdab/sabpred |
| Scrubber 2.0 | BioLogic Software | http://www.biologic.com.au/scrubber.html |
| UCSF Chimera | Pettersen et al., 2004 | https://www.cgl.ucsf.edu/chimera/ |
| UCSF Chimera X | Pettersen et al., 2021 | https://www.cgl.ucsf.edu/chimerax/ |
| GraphPad Prism Software | GraphPad Prism Software, Inc. | N/A |
| PDBePISA | Krissinel and Henrick, 2007 | https://www.ebi.ac.uk/pdbe/pisa/ |
| The PyMOL Molecular Graphics System, v1.8.6 | Schrödinger, LLC | https://pymol.org/2/ |
| IgBLAST-1.16 | Ye et al., 2013 | https://www.ncbi.nlm.nih.gov/igblast/ |
| IMGT | IMGT | http://www.imgt.org/ |
| Python v3.8.3 | Python | https://www.python.org/ |
| The R Project for Statistical Computing | R Core Team | https://www.r-project.org/ |
| R bio3d package | Grant et al., 2006 | http://thegrantlab.org/bio3d/ |

RESOURCE AVAILABILITY

Lead contact

Further information and requests for resources and reagents should be directed to and will be fulfilled by Lawrence Shapiro (lss8@columbia.edu).

Materials availability

This study did not generate new unique reagents.

Data and code availability

- The cryo-EM structures have been deposited to the Electron Microscopy Data Bank (EMDB) and the Protein Data Bank (RCSB PDB). Cryo-EM structural models and maps for antibody 5-7 in complex with SARS-CoV-2 spike have been deposited in the PDB and EMDB with accession codes PDB: 7RW2, EMDB: EMD-24708 respectively.
- This paper does not report original code.
- Any additional information required to reanalyze the data reported in this work paper is available from the Lead Contact upon request.

EXPERIMENTAL MODEL AND SUBJECT DETAILS

Cell lines

FreeStyle 293-F (cat# R79007), Expi293F cells (cat# A14635) were from Thermo Fisher Scientific. HEK293T/17 (cat# CRL-11268), I1 mouse hybridoma (cat# CRL-2700) and Vero E6 cells (cat# CRL-1586) were from ATCC.

FreeStyle 293-F cells and were cultured in serum-free FreeStyle 293 Expression Medium (GIBCO, cat# 12338026) at 37°C, 10% CO₂, 115 rpm. Expi293F cells were cultured in Expi293 Expression Medium (GIBCO, cat# A14635) at 37°C, 8% CO₂, 125 rpm. HEK293T/17 cells and Vero E6 cells were cultured in 10% Fetal Bovine Serum (FBS, GIBCO cat# 16140071) supplemented Dulbecco's Modified Eagle Medium (DMEM, ATCC cat# 30-2002) at 37°C, 5% CO₂. Cell lines were not specifically authenticated.

METHOD DETAILS

Protein samples expression and purification

SARS-CoV-2 S2P spike was produced as described in [Wrapp et al. \(2020b\)](#). Protein expression was carried out in Human Embryonic Kidney (HEK) 293 Freestyle cells (Invitrogen) in suspension culture using serum-free media (Invitrogen) by transient transfection using polyethyleneimine (Polysciences). Cell growths were harvested four days after transfection, and the secreted protein was purified from supernatant by nickel affinity chromatography using Ni-NTA IMAC Sepharose 6 Fast Flow resin (GE Healthcare) followed by size exclusion chromatography on a Superdex 200 column (GE Healthcare) in 10 mM Tris, 150 mM NaCl, pH 7.4.

Biotinylated N-terminal domain of SARS-CoV-2 spike (NTD, residues 1-330) was cloned into the pLEXm mammalian cell expression vector preceded by a BiP signal peptide and in frame with a C-terminal 6X-His tag and an Avi-tag (GLNDIFEAQKIEWHE). The NTD-Avi tag-expression plasmid was transiently co-transfected with the pVRC8400 plasmid encoding the biotin-Ligase BirA from *E. coli* (Lys2-Lys321) into HEK293 cells suspension culture in serum-free media using polyethyleneimine transfectant. The NTD-expression plasmid and BirA plasmid were mixed at a 10:1 ratio for transfection and 3 hr post-transfection the media was supplemented with 50 μM Biotin (Sigma). Media was harvested 4 days after transfection and the secreted protein purified using Ni-NTA IMAC Sepharose 6 Fast Flow resin (Cytiva) followed by size exclusion chromatography (SEC) on Superdex 200 (Cytiva) in 10 mM, Tris pH 7.4, 150 mM NaCl.

NTD-directed monoclonal antibodies 5-7, 4-8, and 5-24 for neutralization assays were expressed and purified as described in [Liu et al., 2020a](#). For SPR experiments, Fabs fragments were produced by digestion of IgGs with immobilized papain at 37°C for 4 h in 50 mM phosphate buffer, 120 mM NaCl, 30 mM cysteine, 1 mM EDTA, pH 7. The resulting Fabs were either purified from Fc by affinity chromatography on protein A (5-7, 4-8) or used as Fab/Fc mixture (5-24).

Monoclonal antibody 5-7 for cryo-EM experiments was expressed and purified as Fab: VHCH1 with a C-terminal His-tag (His₆) and LC were constructed separately into the gWiz expression vector, and then co-transfected and expressed in Expi293. Five days after transfection, supernatants were harvested and 5-7 Fab was purified by nickel affinity chromatography using Ni-NTA agarose (Invitrogen cat# R901-15). Fab purity was assessed by SDS-PAGE; all Fabs were buffer-exchanged into 10 mM Tris, 150 mM, pH 7.4.

Cryo-EM sample preparation

The final sample for EM analysis of the 5-7 in complex with SARS-CoV-2 S2P spike was produced by mixing the Fab and spike in a 1:9 molar ratio, with a final trimer concentration of 0.33 mg/mL, followed by incubation on ice for 1 hr. The final buffer was 10 mM sodium acetate, 150 mM NaCl, 0.005% (w/v) n-Dodecyl β-D-maltoside, pH 4.5. Cryo-EM grids were prepared by applying 2 μL of sample to a freshly glow-discharged carbon-coated copper grid (CF 1.2/1.3 300 mesh); the sample was vitrified in liquid ethane using a Vitrobot Mark IV with a wait time of 30 s and a blot time of 3 s.

Cryo-EM data collection, processing and structure refinement

Cryo-EM data were collected using the Leginon software ([Suloway et al., 2005](#)) installed on a Titan Krios electron microscope operating at 300 kV, equipped with a Gatan K3-BioQuantum direct detection device. The total dose was fractionated for 3 s over 60 raw frames. Motion correction, CTF estimation, particle extraction, 2D classification, *ab initio* model generation, 3D classification and refinements, local refinements and local resolution estimation for all datasets were carried out in cryoSPARC 3.2 ([Punjani et al., 2017](#)); particles were picked using Topaz ([Bepler et al., 2019](#)). Bayesian polishing in RELION was performed on the final set of particles ([Scheres, 2012](#); [Zivanov et al., 2019](#)). Local refinement was carried out using a mask comprising 5-7 Fab and NTD; particles corresponding to the 3-Fabs-bound structure were symmetry-expanded in C3 and merged with the 2-Fabs-bound and the 1-Fab-bound structures for local refinement. Details of the cryo-EM processing workflow are shown in [Figures S2 and S3](#).

SARS CoV-2 S2P spike density was modeled using PDB entry 7L2E ([Cerutti et al., 2021a](#)), as initial template. The initial model for 5-7 Fab variable region was obtained using the SABPred server ([Dunbar et al., 2016](#)). Automated and manual model building were iteratively performed using real space refinement in Phenix ([Adams et al., 2004](#)) and Coot ([Emsley and Cowtan, 2004](#)) respectively. Half maps were provided to Resolve Cryo-EM tool in Phenix to support manual model building. Geometry validation and structure quality assessment were performed using EMRinger ([Barad et al., 2015](#)) and Molprobity ([Davis et al., 2004](#)). Map-fitting cross correlation (Fit-in-Map tool) and figures preparation were carried out using PyMOL, UCSF Chimera ([Pettersen et al., 2004](#)) and Chimera X ([Pettersen et al., 2021](#)). A summary of the cryo-EM data collection, reconstruction and refinement statistics is shown in [Table S1](#).

Authentic SARS-CoV-2 microplate neutralization

The SARS-CoV-2 viruses USA-WA1/2020 (WA1), USA/CA_CDC_5574/2020 (B.1.1.7), hCoV-19/South Africa/KRISP-EC-K005321/2020 (B.1.351), hCoV-19/Japan/TY7-503/2021 (P.1) and hCoV-19/USA/CA (B.1.429) were obtained from BEI Resources (NIAID, NIH) and propagated for one passage using Vero E6 cells. hCoV-19/USA/NY-NP-DOH1/2021 was isolated and sequence was verified (Annavaiah et al., 2021). Virus infectious titer was determined by an end-point dilution and cytopathic effect (CPE) assay on Vero E6 cells as described previously (Liu et al., 2020a).

An end-point dilution microplate neutralization assay was performed to measure the neutralization activity of antibodies. In brief, antibodies were subjected to successive 5-fold dilutions starting from 50 $\mu\text{g}/\text{mL}$. Triplicates of each dilution were incubated with SARS-CoV-2 at a MOI of 0.1 in EMEM with 7.5% inactivated fetal calf serum (FCS) for 1 hour at 37°C.

Post incubation, the virus-antibody mixture was transferred onto a monolayer of Vero E6 cells grown overnight. The cells were incubated with the mixture for ~ 70 hours. CPE of viral infection was visually scored for each well in a blinded fashion by two independent observers. The results were then reported as percentage of neutralization at a given antibody dilution.

Pseudovirus neutralization assays

Plasmids encoding the single and combination mutations found in variants were generated by Quikchange II XL site-directed mutagenesis kit (Agilent). Recombinant Indiana VSV (rVSV) expressing different SARS-CoV-2 spike variants were generated as previously described (Liu et al., 2020a; Wang et al., 2021c). Briefly, HEK293T cells were grown to 80% confluency before transfection with the spike gene using Lipofectamine 3000 (Invitrogen). Cells were cultured overnight at 37°C with 5% CO₂, and VSV-G pseudo-typed ΔG -luciferase (G* ΔG -luciferase, Kerafast) was used to infect the cells in DMEM at a MOI of 3 for 2 hours before washing the cells with 1X DPBS three times. The next day, the transfection supernatant was harvested and clarified by centrifugation at 300 g for 10 min. Each viral stock was then incubated with 20% I1 hybridoma (anti-VSV-G, ATCC: CRL-2700) supernatant for 1 hour at 37°C to neutralize contaminating VSV-G pseudo-typed ΔG -luciferase virus before measuring titers and making aliquots to be stored at -80°C .

Neutralization assays were performed by incubating pseudoviruses with serial dilutions of mAbs or heat-inactivated plasma or sera, and scored by the reduction in luciferase gene expression as previously described (Wang et al., 2021c). Briefly, Vero E6 cells (ATCC) were seeded in 96-well plates (2 \times 104 cells per well). Pseudoviruses were incubated with serial dilutions of the test samples in triplicate for 30 min at 37 °C. The mixture was added to cultured cells and incubated for an additional 16 hr. Luminescence was measured using Luciferase Assay System (Promega), and IC₅₀ was defined as the dilution at which the relative light units were reduced by 50% compared with the virus control wells (virus + cells) after subtraction of the background in the control groups with cells only. The IC₅₀ values were calculated using a five-parameter dose-response curve in GraphPad Prism.

Biliverdin pseudovirus neutralization assays

Pseudovirus was made as described above, neutralization assays were performed by incubating pseudovirus with serial dilutions of 5-7, 4-8 and 5-24 with biliverdin at concentrations 0 μM , 0.2 μM , 1 μM , 5 μM and 10 μM . Pseudovirus was incubated with serial dilutions of mAbs and different biliverdin concentrations in triplicate for 30 min at 37 °C. The mixture was added to cultured Vero E6 cells and incubated for additional 16 hr. Luminescence was measured using Luciferase Assay System (Promega), and IC₅₀ was defined as the dilution at which the relative light units were reduced by 50% compared with the virus control wells (virus + cells) after subtraction of the background in the control groups with cells only. The IC₅₀ values were calculated using a five-parameter dose-response curve in GraphPad Prism.

SPR experiments

SPR binding assays for Fabs 5-7, 4-8 and 5-24 binding to NTD were performed using a Biacore T200 biosensor, equipped with a Series S SA chip, at 25°C. NTD carrying a C-terminal Avi-tag, was captured over a single streptavidin flow cell at approximately 700 RU. A streptavidin surface was used as a reference flow cell to remove bulk shift changes from the binding signal.

Binding experiments for each of the three Fabs binding to NTD were performed in a ligand-free buffer that consisted of HBS-T pH 7.4 (10 mM HEPES pH 7.4, 150 mM NaCl, 0.05% (v/v) Tween-20), and in buffers each supplemented with ligands that have been reported to bind to the NTD hydrophobic pocket such as 1) 0.2 μM biliverdin, 0.5% (v/v) DMSO, 2) 10 μM bilirubin, 1% (v/v) DMSO and 3) 0.01% (v/v) Polysorbate-80 (P-80). Fabs 5-7 and 5-24 were tested using a three-fold dilution series ranging from 1.1-270 nM, and 4-8 was analyzed at concentrations ranging 1.1-90 nM, using also a three-fold dilution series. Each Fab was tested in order of increasing protein concentration, in duplicate. The association and dissociation rates were each monitored for 120 s and 600 s respectively, at 50 $\mu\text{L}/\text{min}$. The NTD surface was regenerated using two-consecutive 10 s pulse of 15 mM H₃PO₄ at a flow rate of 100 $\mu\text{L}/\text{min}$, followed by a 60 s buffer wash at the same flow rate. Blank buffer cycles were performed by injecting running buffer instead of Fab to remove systematic noise from the binding signal. The data was processed and fit to 1:1 interaction model using the Scrubber 2.0 (BioLogic Software).

Antibody gene assignments and genetic analyses

The 13 NTD-directed SARS-COV-2 neutralizing and 1 non-neutralizing antibodies were collected from six publications. We annotated these antibodies using IgBLAST-1.16.0 with default parameters (Ye et al., 2013). For antibody 5-7, the N-addition, D gene,

and P-addition regions were annotated by IMGT V-QUEST (Brochet et al., 2008). The gene specific substitution profile of IGHV1-46 and IGKV1-9 were download from cAb-Rep database (Guo et al., 2019).

Sequence entropy comparison

The residues of 5-7 paratope were obtained by PDBePISA (Krissinel and Henrick, 2007), with the default parameters. Per residue sequence entropy was download from the next strain database (Hadfield et al., 2018), which enabled by data from GISAID (<https://www.gisaid.org/>). The p value among different paratope groups were calculated by Kolmogorov–Smirnov test in R, with the significant level set as $p < 0.05$. The geometric mean and 95% CI of per residue sequence entropy were calculated and plotted by GraphPad Prism version 9. The visualization of sequence entropy was displayed by PyMOL version 2.3.2.

QUANTIFICATION AND STATISTICAL ANALYSIS

The statistical analyses for the pseudovirus neutralization assessments were performed using GraphPad Prism. Cryo-EM data were processed and analyzed using cryoSPARC and RELION. The SPR data were fitted using Biacore Evaluation Software and Scrubber. Cryo-EM and crystallographic structural statistics were analyzed using Phenix, Molprobit, EMringer and Chimera. The correlations were performed in R. Statistical details of experiments are described in [Method details](#) or figure legends.